



1 **Assessing the perturbations of the hydrogeological regime in** 2 **sloping fens through roads**

3 Fabien Cochand¹, Daniel Käser¹, Philippe Grosvernier², Daniel Hunkeler¹, Philip Brunner¹

4 ¹Centre of Hydrogeology and Geothermics, Université de Neuchâtel, Switzerland.

5 ²LIN'eco, ecological engineering, PO Box 51, 2732 Reconvilier, Switzerland.

6

7 Corresponding author: Fabien Cochand, fabien.cochand@unine.ch

8 **Abstract**

9 Roads in sloping fens constitute a hydraulic barrier for surface and subsurface flow. This can lead to a
10 drying out of downslope areas of the sloping fen as well as gully erosion. Different types of road construction have
11 been proposed to limit the negative implications of the roads on flow dynamics. However, so far no systematic
12 analysis of their effectiveness has been carried out. This study presents an assessment of the hydrogeological
13 impact of three types of road structures in semi-alpine, sloping fens in Switzerland. Our analysis is based on a
14 combination of field measurements and fully integrated, physically based modelling. In the field approach, the
15 influence of the road was examined through tracer tests where the upslope of the road was sprinkled with a saline
16 solution. The spatial distribution of electrical conductivity downslope provided a qualitative assessment of the
17 flow paths and thus the implications of the road structures on subsurface flow. A quantitative albeit not site-specific
18 assessment was carried out using numerical models simulating surface and subsurface flow in a fully coupled way.
19 The different road types were implemented in the model and flow dynamics were simulated for a wide range of
20 slopes and hydrogeological conditions such as different hydraulic conductivity of the soil. The results of the field
21 and modelling analysis are coherent. Roads designed with an L-drain collecting water upslope and releasing it in
22 a concentrated manner downslope constitute the largest perturbations. The other investigated road structures were
23 found to have less impact. The developed methodologies and results are useful for the planning of future road
24 projects.



25 1 Introduction

26 Wetlands can play a significant role in flood control (Baker, 2009;Zollner, 2003;Reckendorfer, 2013),
27 mitigate climate change impacts (Cognard Plancq et al., 2004;Samaritani et al., 2011;Lindsay, 2010;Limpens,
28 2008) and feature great biodiversity (Rydin, 2005). However, the world has lost 64% of its wetland areas since
29 1900 and an even greater loss has been observed in Switzerland (Broggi, 1990). Therefore, wetland conservation
30 has received considerable attention. However, the sprawl of human infrastructure, land use changes, climate
31 change or river regulations remain serious factors that threaten wetlands. For instance, roads can substantially
32 modify the surface-subsurface flow patterns of sloping fens. The changes in flow patterns can influence sediment
33 transport, moisture dynamics and biogeochemical processes as well as ecological dynamics.

34 The link between hydrological changes and sediment dynamics has been studied in various contexts. From
35 a civil engineering perspective, erosion of the road must be avoided. A common strategy to avoid erosion of the
36 road foundation is to collect water in drains and then release it in a concentrated manner downslope. This, however,
37 can lead to erosion of the downslope area, a phenomenon known as « gully erosion ». A number of studies
38 specifically focused on identifying the controlling processes and relevant parameters of gully erosion (Capra et al.
39 (2009);Valentin et al. (2005);Descroix et al. (2008);Poesen et al. (2003);Martínez-Casasnovas (2003);Daba et al.
40 (2003);Betts and DeRose (1999);Derose et al. (1998), among others). Nyssen et al. (2002) investigated the impact
41 of road construction on gully erosion in the northern Ethiopian highlands, with a focus on surface water. In their
42 study area, they observed the formation of a gully after the road construction downslope culvert and outlets of
43 lateral road drains. Based on fieldwork and a subsequent statistical analysis, they concluded that the main causes
44 for gully development are the concentrated runoff, the diversion of centered runoff to other catchments and the
45 modifications of drainage areas induced by the road. The role of groundwater was not considered in this study.

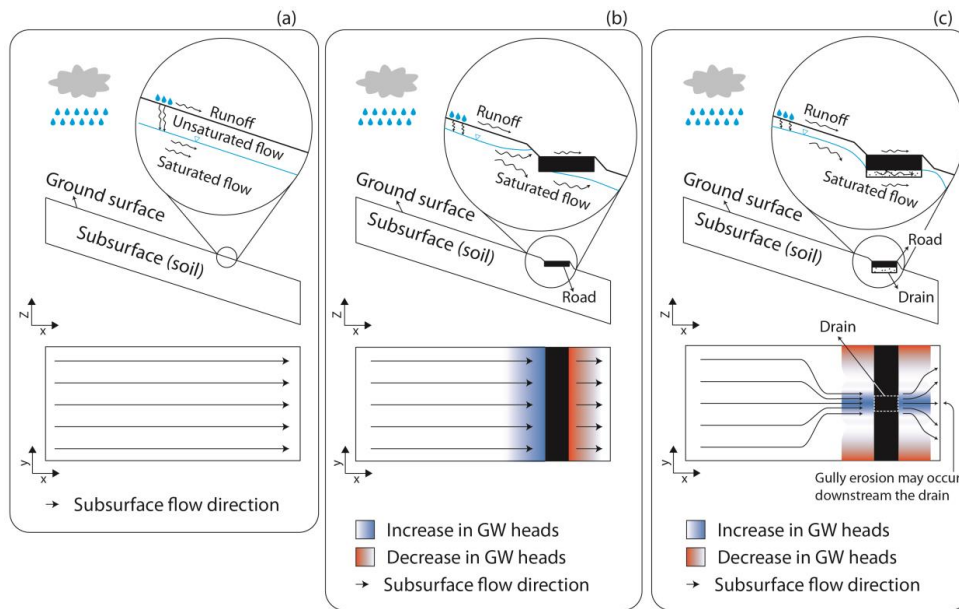
46 Reid and Dunne (1984) developed an empirical model for estimating road sediment erosion of roads located
47 in forested catchments in the Washington state (USA). They concluded that a heavily used road produced 130
48 times more sediment than an abandoned road. Wemple and Jones (2003) also developed an empirical model for
49 estimating runoff production of a forest road at a catchment scale. They demonstrated that during large storm
50 events, subsurface flow can be intercepted by the road. The intercepted water, if directly routed to ditches, increases
51 the rising limb of the catchment hydrograph. At a smaller spatial scale (0.1 km²) Loague and VanderKwaak (2002)
52 assessed the impact of a road on the surface and subsurface flow using an integrated surface-subsurface flow model
53 InHM (Integrated Hydrology Model) (VanderKwaak, 1999) in a rural catchment. The results showed that the road



54 induced a slight increase of runoff and a decrease of surface-subsurface water exchange around the road. Dutton
55 et al. (2005) investigated the impact of roads on the near-surface subsurface flow using a variability saturated
56 subsurface model. They concluded that the permeability contrast caused by the road construction leads to a
57 disturbance of near-surface subsurface flow which may significantly modify the physical and ecological
58 environment.

59 Road construction can also impact the development of vegetation (Chimner, 2016). von Sengbusch (2015)
60 investigated the changes in growth of bog pines located in a mountain mire in the black forest (south-west
61 Germany). The author suggests that the increase of bog pine cover is caused by a delayed effect of a road
62 construction in 1983 along a margin of the bog. The road affects subsurface flow and therefore prevents the upslope
63 water to flow to the bog. According to von Sengbusch (2015), the road disturbances induce a larger variability in
64 water table elevations during dry periods and consequently increase the sensitivity of the bog to climate change.

65 Based on these previous studies and basic principles of subsurface flow, a simple conceptual model
66 describing the influence of roads on the flow system can be drawn (Figure 1). Roads are generally built with
67 materials of low hydraulic conductive and therefore act as a hydrogeological barrier. In natural conditions,
68 rainwater infiltrates the soil and follows the topographical gradient. In case of heavy precipitation events, water
69 can also directly flow on the surface (Figure 1a). If a road is constructed, it constitutes a hydrogeological barrier
70 (Figure 1b) and consequently affects the flow dynamics. Drains installed underneath the road Figure 1c) can
71 mitigate the effect of this hydrogeological barrier. The design and the materials of drains significantly affect flow
72 dynamics. Figure 1c presents a typical condition where a non-continuous drain (i.e., drains are perpendicularly
73 installed at regular distances along the road) is used to connect both sides of the road. Upstream and downstream
74 subsurface flows are deviated and the drain becomes the main outlet. The concentration of subsurface flow
75 downstream of the drain may induce gully erosion and disturb the hydraulic regime of the sloping fens.



76

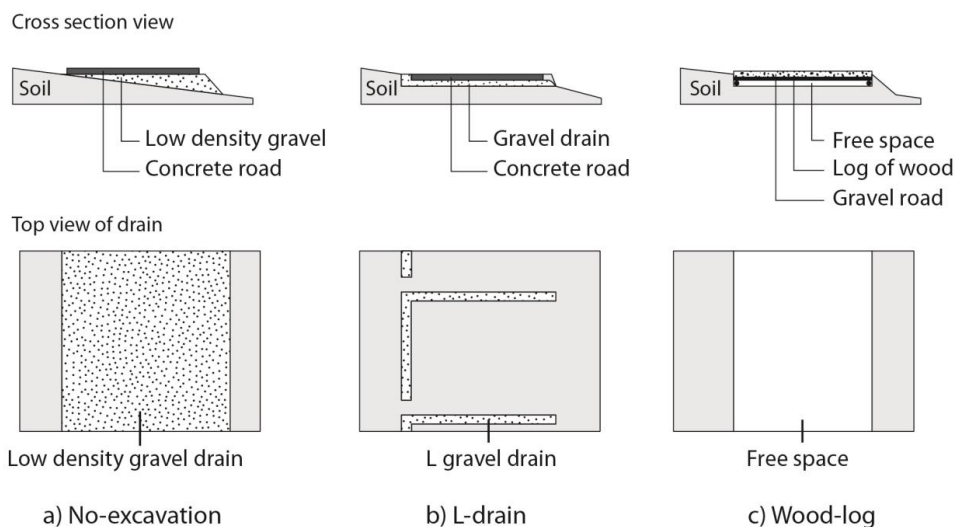
77 **Figure 1 Conceptual subsurface dynamics in sloping fens: a) natural conditions, b) with road without a drain and c)**
 78 **with a road and a drain.**

79 While these studies clearly indicate that roads can have adverse effects on the surface and subsurface flow
 80 dynamics and the associated ecosystems, a detailed study on how roads perturb the flow system and dynamics in
 81 a sloping fen has not been carried out. In Switzerland, more than 20'000 ha are included in the national inventory
 82 of fens of national importance (Broggi 1990), most of them are located in the mountainous regions of the northern
 83 Prealps. Hence, the majority of Swiss fens is composed of sloping fens, which developed on nearly impermeable
 84 geomorphological layers such as silty moraine material or a particular rock layer named “flysch”. Although
 85 organic, soils are not necessarily peaty and most of the time quite superficial, not exceeding a few decimeters in
 86 thickness. Water flow is therefore mostly consisting of runoff and partly occurring in the shallow part of the
 87 subsurface. The construction of a road in this kind of sloping fens removes completely the soil layer in which
 88 subsurface flow occurs, thus constituting a major perturbation of the hydraulic regime. Construction techniques to
 89 limit these adverse impacts have been proposed but their efficiency has so far not been investigated. Three road
 90 structures with various construction techniques and materials (hereinafter further detailed) were developed in
 91 Switzerland to reduce impacts of roads. These road types are conceptually illustrated in Figure 2. The efficiency
 92 of developed road structures was so far not assessed after completion. This study focuses on these three road
 93 structures described hereafter:



- 94 • The *no-excavation* structure (Figure 2a) aims at preserving soil continuity under the road. It consists of a
95 levelled layer of gravel, anchored to the ground, and underlying 0.16 m thick concrete slabs. Soil
96 compaction is limited by using a low-density gravel, made of expanded glass chunks (Misapor™) -
97 approximately fivefold lighter than conventional material.
- 98 • The *L-drain* structure (Figure 2b) aims at collecting subsurface water upstream the road and redirecting
99 it to discrete outlets on the other side. The setup consists of a trench, approximately 0.4 m deep, filled
100 with a matrix of sandy gravel that contains an L-shaped band of coarse gravel acting as the drain.
- 101 • The *wood-log* structure (Figure 2c) aims at promoting homogeneous flow under the road but does not
102 preserve soil continuity. Embedded in a trench, approximately 0.4 m deep, the wooden framework is
103 filled with wooden logs forming a permeable medium. The wooden logs are then covered with mixed
104 gravel.

105 The aim of this study is to investigate, document and assess the hydrogeological impact of various road
106 structures and their effects on fen water dynamics. A combination of fieldwork and hydrogeological modelling
107 tasks was employed. Fieldwork was used to document and obtain the required information on the hydrogeological
108 impact of existing road structures on fen water dynamics. Sites with similar natural conditions were chosen to
109 compare the influence of different road constructions on flow processes. The field studies allow for assessing the
110 effectiveness of a given road structure, however, they cannot provide generalizable analysis of the different road
111 types under different environmental and physical conditions, e.g. the slope or the hydraulic properties of the fen.
112 This gap was filled by the development of generic numerical models. The main advantage of the modelling
113 approach is the possibility to generate a multitude of different models with various characteristics such as different
114 road structures, slopes or fen hydraulic conductivity and to test their impacts on the flow dynamics.



115

116 **Figure 2 : Conceptual road structures, a) No-excavation road structure, b) L-drain road structure and c)**
117 **Wood-log road structure.**

118 2 Methods

119 2.1 Study areas and fieldwork

120 Four sloping fen areas located in alpine or peri-alpine regions of Switzerland (Table 1) were selected. All
121 areas are situated in protected fen areas, and their selection was based on two main criteria:

- 122 1. The subsurface water flow must occur only in the topsoil layer and as runoff (as described in the
123 introduction).
- 124 2. The types of installed road structures (no-excavation, L-drain and wood-log).

125 To fulfil the first criteria, soil profiles were analysed to ensure that each area with different road types had the
126 same soil stratigraphy: It had to be composed of organic soil on top of a layer of impermeable clay and similar
127 hydraulic regimes (e.g., runoff and subsurface flow occurring only in the topsoil layer). In addition, to ensure that
128 subsurface water is forced to cross the road instead of flowing in parallel of the road (and thus not being affected
129 directly by the road), another important criterion for the selection of the study areas was that subsurface flows
130 perpendicular to the road.

131 To evaluate the hydraulic connection provided by the road structures, tracer tests were carried out. As
132 illustrated schematically in Figure 3, a saline solution was spread on the upslope area and the occurrence of the



133 tracer was monitored downslope the road. In the absence of surface runoff, the occurrence of a tracer downslope
134 demonstrates the hydrogeological connection through the road. Furthermore, the spatial distribution of the tracer
135 front reflects the heterogeneity of the flow paths.

136 **Table 1. Field site locations and features.**

	St-Antonien (STA)	Schoeniseiswand (SCH)	Stouffe (STO)	Höhmad (HMD)
<i>Road type</i>	No excavation	L-Drain	Wood-log	Wood-log
<i>Terrain slope</i>	0.27	0.13	0.13	0.15
<i>WGS84 coordinates</i>	46.96760°N 9.84843°E	46.78872°N 7.96805°E	46.72957°N 7.83861°E	46.74027°N 7.89871°E

137

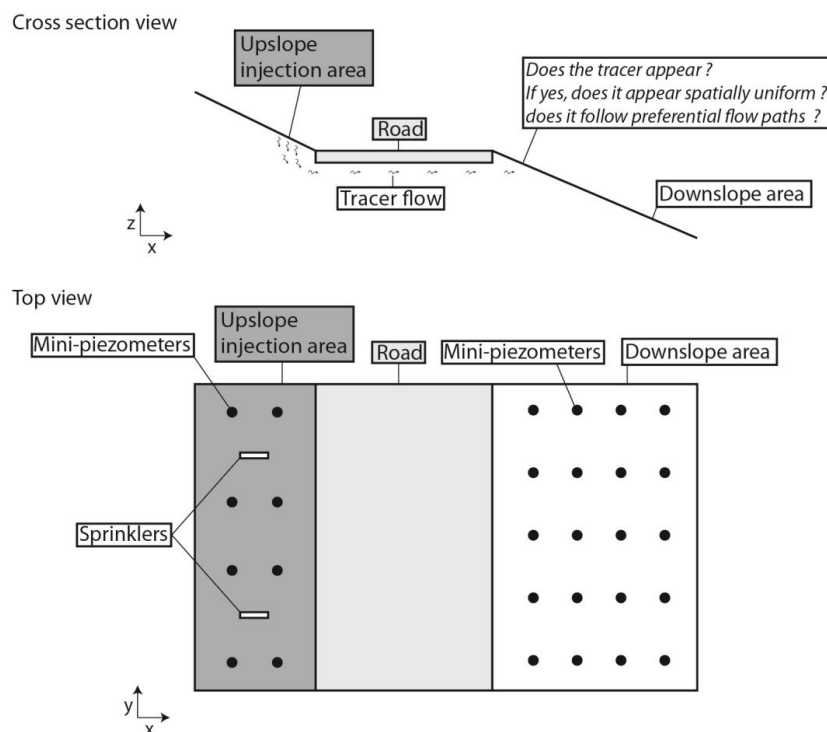
138 Each area corresponds to an 8 x 20 m rectangle that includes a 2.5 to 3.5 m wide road segment. A network
139 of approximately 30 mini-piezometers on both sides of the road (Figure 3) was installed to monitor the hydraulic
140 heads and was used to obtain samples for the tracer test.

141 The mini-piezometers are high-density polyethylene (HDPE) tubes no longer than 1.5 m (ID: 24 mm). Each
142 tube was screened with 0.4 mm slots from the bottom end to 5 cm below ground level. It was inserted into the soil
143 after extracting a core with a manual auger (diameter: 4-6 cm). The gap between the tube and the soil was filled
144 with fine gravel and sealed on the top with a 4 cm thick layer of bentonite or local clay. Hydraulic heads were
145 measured using a manual water-level meter (± 0.3 cm). At each point, the terrain and the top of the piezometer
146 were levelled using a level (± 0.3 cm), whereas the horizontal position was measured with a tape measure (± 5
147 cm).

148 The tracer tests were conducted using two oscillating sprinklers designed to reproduce a 30 mm rain event
149 during 2-3 hours. This is equivalent to an intense rain event. Prior to the experiment, the sprinklers were activated
150 for 15-60 minutes to wet the soil surface. Sodium chloride was added to the irrigated solution to obtain an electrical
151 conductivity of 5-10 mS/cm which is approximately ten times higher than the natural electrical conductivity of the
152 groundwater. Then, the area (60 m²) upslope of the road (upslope injection area of Figure 3) was irrigated with the
153 salt solution using the two sprinklers. The electrical conductivity (EC) of soil water was manually measured using
154 a conductimeter in all mini-piezometers prior to the experiment, immediately after, and 24h later. An increase in
155 EC in piezometers located in the downslope area indicates that the injected salt water flowed from the upslope
156 area to the downslope area below the road and indirectly indicates a hydraulic connection. Conversely, if no



157 changes in EC are observed in piezometers, this indicates that there is no connection below the road and finally a
158 decrease in EC is not expected.



159

160 **Figure 3 : Schematic view of the fieldwork areas.**

161 2.2 Numerical modelling

162 To simulate and quantify the impact of the roads on the flow dynamics in sloping fens, the modelling
163 approach was structured in three steps. First, a 3D base case model representing surface and variably saturated
164 subsurface water flow in a sloping fen was elaborated. Then, the base case model was modified to represent the
165 three different types of investigated road structures. For each model, various slopes, organic soil and road drain
166 hydraulic conductivities were implemented to produce a sensitivity analysis and explore their sensitivities in the
167 sloping fen flow dynamics (see section 2.2.3 for details). Finally, a comparison of all model results was made in
168 order to assess the impact of road structures and quantify the dynamics and the physical controls of subsurface
169 flow in these environments.

170 **2.2.1 Numerical simulator**

171 The model used in the study is HydroGeoSphere (HGS) (Therrien et al., 2005). HGS is a physically-based
172 surface–subsurface fully-integrated model using the control volume finite element approach. HGS simultaneously
173 solves a modified Richards' equation (Eq. 1) describing the saturated and unsaturated 3D subsurface flow and the
174 2D depth average diffusion-wave approximation of the Saint Venant equation (Eq. 3) for describing the surface
175 flow. Richard's equation is given as:

$$-\nabla \cdot (q) \pm Q_s + \sum \Gamma_{ex} = \frac{\partial}{\partial t} (\theta_s S_w) \quad \text{Eq. 1}$$

176 where $\nabla = \partial/\partial x, \partial/\partial y, \partial/\partial z$, Q_s represents fluid exchanges with the outside of the simulation domain (*e.g.*
177 injection wells), $\sum \Gamma_{ex}$ is the volumetric fluid exchange rate between the subsurface domain and all other simulation
178 domains supported by HGS (surface domain, tile drain domain, among others), θ_s is the porosity, S_w is the water
179 saturation and q is the Darcy flux (Eq. 2) of water given as:

$$q = K \cdot k_r \nabla (\psi + z) \quad \text{Eq. 2}$$

180 Where K is the hydraulic conductivity of the subsurface ψ is the pressure head of water, z is the elevation and k_r
181 is the relative hydraulic conductivity. k_r varies between 1 when the domain is fully saturated and near zero when
182 the domain is fully unsaturated. The Van Genuchten (1980) functions which relate pressure head to saturation and
183 relative hydraulic conductivity is employed. For surface flow, the diffusion-wave approximation of the Saint
184 Venant equation (Eq. 3) is given as:

$$\frac{\partial \phi_o h_o}{\partial t} - \frac{\partial}{\partial x} \left(d_o K_{ox} \frac{\partial h_o}{\partial x} \right) - \frac{\partial}{\partial y} \left(d_o K_{oy} \frac{\partial h_o}{\partial y} \right) + d_o \Gamma_o \pm Q_o = 0 \quad \text{Eq. 3}$$

185 where ϕ_o is the surface porosity varying between zero at the ground surface and unity at the top of a rill or
186 obstruction, h_o is the surface water elevation, d_o surface water depth ($h_o = d_o + z$), Q_o is a volumetric flow rates
187 representing external source and sinks, K_{ox} and K_{oy} are surface conductance (Eq. 4) given as:



$$K_{ox,y} = \frac{d_o^{2/3}}{n_{x,y}} \frac{1}{(\partial h_o / \partial s)^{1/2}} \quad \text{Eq. 4}$$

188 where $n_{x,y}$ are the Manning roughness coefficients in the x and y directions and s is the slope taken in the direction
189 of maximum slope. Finally, the term Γ_o represents fluid exchanges with other domains. The water exchanges
190 between the surface and subsurface domains are calculated using the “dual node approach” (Eq. 5) and is given
191 as:

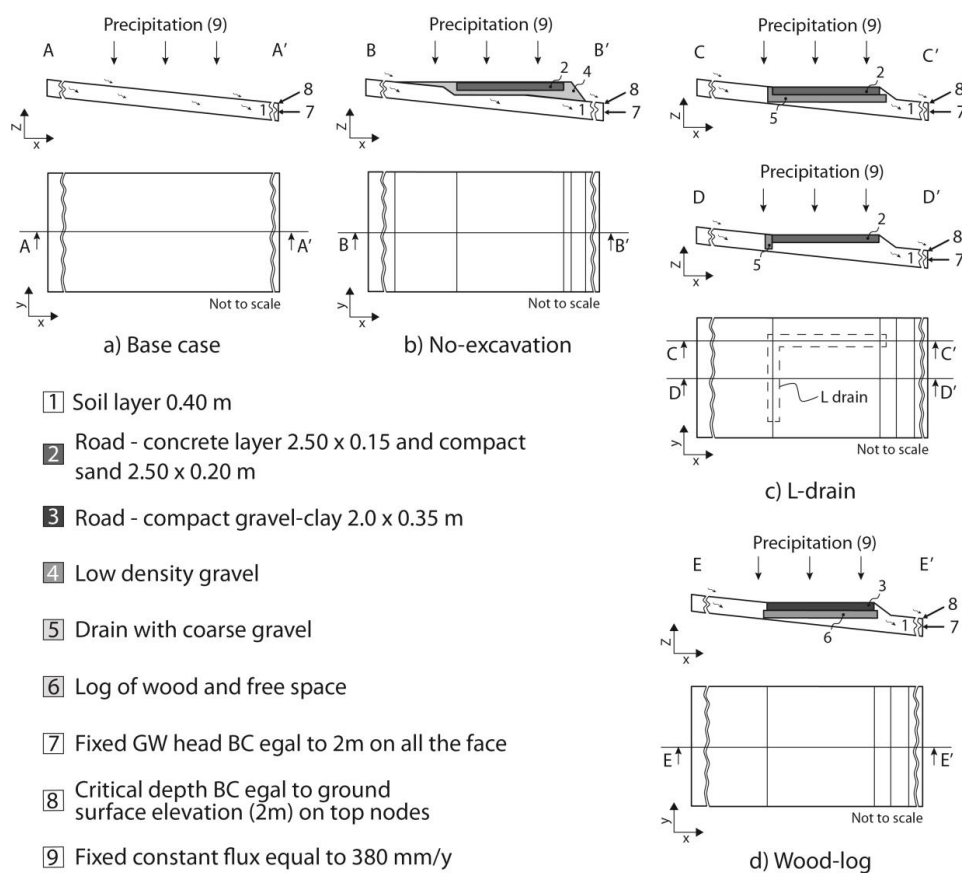
$$d_o \Gamma_o = \frac{k_r K_{zz}}{l_c} (h - h_o) \quad \text{Eq. 5}$$

192 In this approach, the top nodes representing the ground surface are used for calculating both subsurface and surface
193 flow. The water exchanges are calculated as hydraulic head differences of the two domains represented by $h - h_o$
194 and multiplied by the vertical hydraulic conductivity of the top layer, $k_r K_{zz}$, and a coupling factor, (l_c).

195 The iterative Newton-Raphson method is used to solve the nonlinear equations. At each subsurface node, saturation
196 and groundwater heads are calculated, which allows for the calculation of the Darcy flux. On the surface domain,
197 the surface water heights are calculated at each node to determine surface water flux. Rivers and lakes are
198 characterized by a surface water depth larger than 0. For further details on the code and HGS capabilities, see
199 Therrien et al. (2005), Li et al. (2008) or Brunner and Simmons (2012).

200 2.2.2 Conceptual models and model implementation

201 Figure 4 illustrates the conceptual model of each case. Geometry, topography and slopes are based on the
202 physical conditions in the field. In each model, the soil layer has a thickness of 0.4 m and the surface and subsurface
203 water are only supplied by precipitation. The upstream boundary is the catchment boundary (water divide) and the
204 downstream boundary represents the outlet of the model. Finally, it was assumed that the layer beneath the soil
205 was impermeable (as observed in the field) and engineering plans were used to design drain and road. One
206 Neumann (constant flux) boundary condition was used on the top face for simulating precipitation. A constant
207 groundwater head boundary condition (Dirichlet type) equal to the ground surface elevation (2m) was used on the
208 right face ($x=76$ m on the Figure 5a) allowing the groundwater to flow out of the model. Finally, a critical depth
209 boundary condition which forces the surface water to reach a given elevation (2 meters in our case) to flow out of
210 the model was implemented on the top nodes located at $x=76$ m and all other faces are no flow boundary conditions.



211

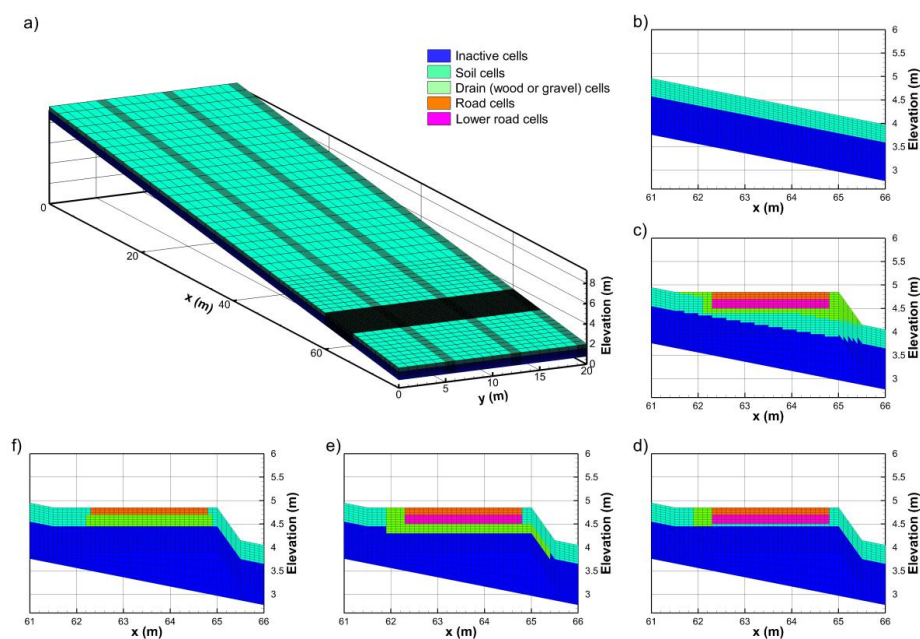
212 **Figure 4 : a) Base case, b) No-excavation, c) L-drain and d) Wood-log structures conceptual models.**

213 To numerically solve the 3D flow equation, a 3D mesh was developed (Figure 5a). The mesh is 76 m long
 214 in the X direction, 20 m in the Y direction and the mesh thickness is 1.2 m. The top elevation was fixed at 2 m on
 215 the right side ($x=76\text{m}$) and varies from 9.6 m to 24.8 m on the left side ($x=0$) according to the slope of the model.
 216 The mesh was made up of 24 layers, 127,200 nodes and 118,440 rectangular prism elements. To ensure an
 217 appropriate level of detail, several mesh discretization refinements were made. Therefore, the element size varies
 218 between 2m and 0.1 m horizontally (in the X and Y directions) and 0.09 m and 0.05 m vertically.

219 The base case model and the three other models representing different road types have the same boundary
 220 conditions and finite element meshes, however, modifications were made between coordinates $61 < x < 66$
 221 to implement the different road types. Figure 5 depicts the differences between the base case model (Figure 5a and
 222 b) and models with roads (Figure 5c, d, e and f). In the case of models with a road, the mesh was deformed and



223 the properties were changed. The fine spatial discretization of the mesh created between the coordinates $61 < x < 66$
 224 allows a more accurate representation of the simulated processes where high hydraulic gradients are expected (near
 225 roads and drains). Additionally, the refinements allow an accurate representation of drains and the roads.



226

227 **Figure 5 : Model development: a) Base case model, b) Base case model cross-section between $61m < x < 66m$, c) No-**
 228 **excavation model between $61m < x < 66m$, d) L-drain model between $61m < x < 66m$, e) L-drain model between $61m <$**
 229 **$x < 66m$ along the transversal drain f) Wood-log model between $61m < x < 66m$.**

230 2.2.3 Sensitivity analysis

231 The sensitivity analysis consists of the variation of model properties and parameters in order to understand
 232 how they control the sloping fen dynamics. The sensitivities of the following parameters were analyzed: fen slope,
 233 soil hydraulic conductivities and road drain hydraulic conductivities. For each property, three different values were
 234 selected and are summarized in Table 2. The soil hydraulic conductivities vary between 8.64 [m/d] and 0.0864
 235 [m/d] to represent all ranges of observed soil hydraulic conductivities (Charman, 2002). The road drains hydraulic
 236 conductivities vary between 8640 [m/d] and 86.4 [m/d] which correspond to very coarse and coarse gravel. Finally,
 237 the slopes were fixed at 10%, 20% and 30% as observed during the fieldwork. Note that the drain hydraulic
 238 conductivities of the wood-log (W-L) were assumed ten times more conductive and more porous than gravel drain
 239 because of its particular structure (wood logs). In order to simulate each parameter combination, a total of 90
 240 models were developed (27 models for each road structures and 9 models for natural conditions).



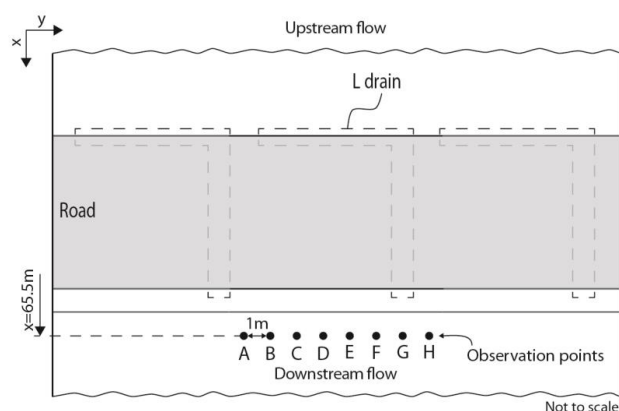
241 **Table 2 : Subsurface and surface flow parameters.**

Subsurface flow properties					
	Hydraulic conductivity	Porosity	Van Genuchten α	Van Genuchten β	Residual water content
Units	K [md ⁻¹]	θ [-]	α [m ⁻¹]	β [-]	Swr [-]
Soil - KS1	8.64	0.25	4	1.41	0.04
Soil - KS2	0.864	0.25	4	1.41	0.04
Soil - KS3	0.0864	0.25	4	1.41	0.04
Drains - KD1	8640	0.25	29.4	3.281	0.04
Drains - KD2	864	0.25	29.4	3.281	0.04
Drains - KD3	86.4	0.25	29.4	3.281	0.04
Drains - WL - KD1	86400	0.7	29.4	3.281	0.04
Drains - WL - KD2	8640	0.7	29.4	3.281	0.04
Drains - WL - KD3	864	0.7	29.4	3.281	0.04
Road concrete	0.0000864	0.05	1.581	1.416	0.04
Road fine sand	0.00864	0.25	4	1.416	0.04

Surface flow properties					
	Coupling length	Manning's roughness coefficient		Rill storage height	Obstruction height
Units	l_c [m]	n_x [m ^{-1/3s}]	n_y [m ^{-1/3s}]	D_t [m]	O_t [m]
Soil	1. x 10 ⁻²	0.03	0.03	0.005	0.005
Road	1. x 10 ⁻²	0.018	0.018	0.001	0.001

242

243 Models are run for 10⁷000 days (about 27 years) with a constant flux equal to 380 mm/y on the top
 244 representing the rainfall to reach a steady state. This precipitation allows for the saturation of the downslope part
 245 of the model. Subsequently, subsurface water velocities in the soil layer were extracted at each observation point
 246 located downslope from the road (Figure 6). The subsurface water velocities are proportional to the volumetric
 247 groundwater flow and consequently, changes in groundwater velocity indicate a perturbation of flow dynamics.
 248 Therefore, a comparison of velocities between each model was made to present the effect of each road structure
 249 and sloping fen properties on the dynamics.



250

251 **Figure 6 : Location of observation points in the models.**

252 **3 Results and Discussion**

253 **3.1 Fieldwork**

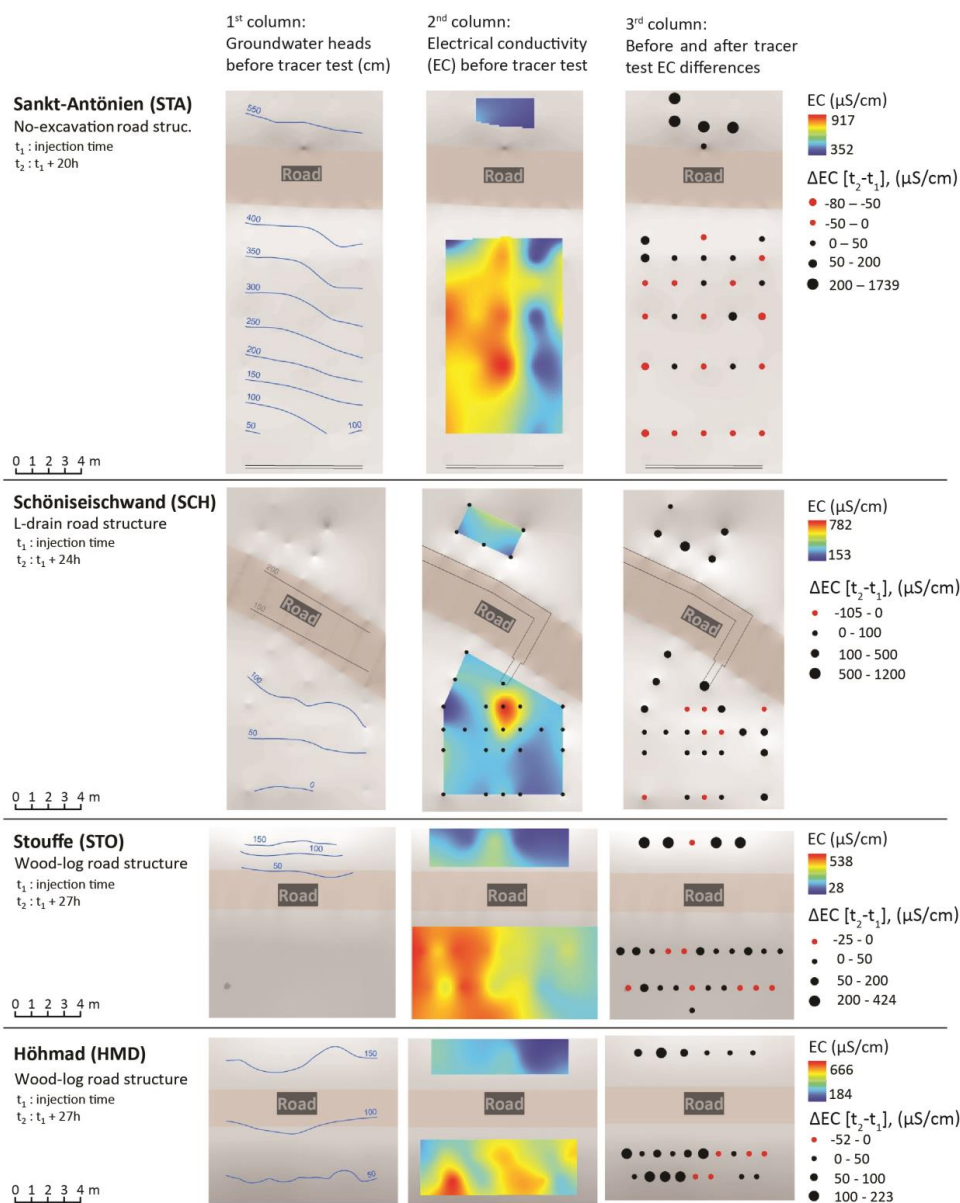
254 Based on the observations, all sites show a continuous saturated zone before the experiment, both upstream and
255 downstream of the road, the hydraulic gradients being mostly similar to the terrain slope (Figure 7, 1st column).
256 In contrast, the EC maps established prior to the tracer test show spatial variability at a length scale of one to
257 several meters (Figure 7, 2nd column.). Within each plot, EC varies from 482 to 629uS/am. At the SCH site, the
258 highest values are located downstream of the L-drain outlet which could indicate that the EC increases as water is
259 flowing through the drain (e.g. through the dissolution of the construction material). Given that this initial
260 distribution of EC is not uniform, the comparison of EC after the sprinkling experiment has to be made in a relative
261 manner (Figure 7, 3rd column).

262 The heterogeneity of the hydraulic conductivity of the soil is apparent from the tracer test results (Figure 7,
263 3rd column: EC 24 hours after injection). At all four sites, the front of the saline solution is not uniform but follows
264 the heterogeneity of the soil hydraulic conductivity. Nevertheless, road structures may play the role of a
265 preferential flow path that is particularly obvious at the SCH site where the front follows two preferential flow
266 paths. One related to the L-drain (right path) and the other on the left, unrelated to the L-drain, suggesting that the
267 latter drains only a part of the water and the other part follows a natural preferential flow path. At the HMD site,
268 the saline solution is far more concentrated on the left side of the plot, yet apparently not as a result of the road's
269 structure. Rather, the soil appears more permeable on the left side of the plot, both upslope and downslope of the
270 road. Finally, the decrease in EC observed 24 hours after injection at some locations might result from the



271 following: (1) the tracer injection induces, by “piston effect”, the displacement of a small volume of local water
272 with a lower EC; (2) the tracer injection was preceded by a period of irrigation without tracer, which could have
273 diluted the pre-irrigation soil solution.

274 In each case, the irrigation experiments demonstrate the continuity of subsurface flow under the road for
275 all structures. For the no-excavation and wood-log type, the perturbation of the flow field seems controlled by the
276 natural heterogeneity of the soil and flow paths, and not by the road itself. Conversely, the field data strongly
277 suggest that the L-drain constitutes an important preferential pathway and consequently subsurface flow is
278 increasingly concentrated. In terms of wetland conservation, this flow convergence is a serious threat (gully
279 erosion, local drying up of the soil). Despite these strong indications, it is clear that with the field data alone no
280 conclusive analysis can be made as no data before the construction of the road are available. Fieldwork allows for
281 site-specific conclusions, but more general conclusions which are not specific to a site are impossible. Therefore,
282 numerical modelling was used to fill this gap.



283

284 **Figure 7 : Fieldwork results at the four field sites: 1st column) Measured groundwater heads before tracer test, 2nd**
 285 **column) Measured EC before tracer test and 3rd before and after tracer test differences in EC.**

286



287 3.2 Modelling

288 Figure 8 shows the results of the models with a slope of 10%, Figure 9 with a slope of 20% and Figure 10
289 with a slope of 30%. In each dot chart, the groundwater velocities (always in m/d) are plotted with crosses for the
290 base case model, diamonds for the no-excavation type, squares for the L-drain type and circles for the wood-log
291 type. In following paragraphs, the base case (natural conditions) results are presented and discussed, followed by
292 the simulations of the road structures. Finally, all model results are discussed.

293 In the base case model, groundwater velocities vary from 0.013 (m/d) to 0.269 (m/d) for 10% slope, 0.025
294 (m/d) to 0.269 (m/d) for 20% slope and to 0.038 (m/d) to 0.274 (m/d) for 30% slope. The groundwater velocity
295 decreases gradually depending on the hydraulic conductivities (KS) of the soil layer. For any slope, where
296 hydraulic conductivities are high (KS1), groundwater velocities are higher compared to the case where hydraulic
297 conductivities are low (KS3). The primary observation is that groundwater velocities are mainly controlled by the
298 hydraulic conductivities and therefore the slope plays a minor role. Differences between the maximum and
299 minimum hydraulic conductivity are two orders of magnitude, whereas changes between slopes are very small.
300 The main effect of slope is to slightly increase groundwater velocities when the hydraulic conductivities are low
301 (0.0864 m/d) due to the increase of the topographic gradient.

302 In the no-excavation and wood-log type models, the effect of road structures is quite similar. The
303 groundwater velocities vary from 0.028 (m/d) to 0.269 (m/d) for 10% slope, 0.025 (m/d) to 0.269 (m/d) for 20%
304 slope and 0.042 (m/d) to 0.269 (m/d) for 30% slope. Compared to the base case model, results show that the no-
305 excavation and wood-log type structures have a minimal impact. The only marked difference is that groundwater
306 velocities are slightly higher if the hydraulic conductivities are low (KS3) for each slope in the wood-log type
307 model. This can, to a certain extent, be explained by the fact that the hydraulic conductivity of the base of the road
308 (consisting of wood-logs) is higher than the hydraulic conductivity of the soil and therefore facilitate the
309 infiltration. Conversely, in the base case model, less water is infiltrated but more runoff occurs. For the no-
310 excavation model with a slope of 10%, results are not presented for technical reasons. For this specific geometry
311 and topography, a different structure of the mesh had to be generated which did not allow for a direct visual
312 comparison with the other models. In the 20% and 30% slope models, the results of the no-excavation model are
313 similar to the base case model.

314 In the L-drain type model, the effect is markedly different from the other road structures. The groundwater
315 velocities vary significantly in the observation points. The maximum velocities are always obtained in the



316 observation point G just downstream the drain outlet and may be 10 times higher than in the base case. Conversely,
317 minimum velocities are obtained in C and D observation points in which velocity may be 10 times lower.
318 Significant differences in groundwater velocity are also observed in the same transect. The maximum differences
319 are observed if the hydraulic conductivity of soil (KS) and drain (KD) are high and may vary from to 0.017 (m/d)
320 to 1.281 (m/d). Conversely, when KS and/or KD are low, the differences along the transect are smaller. The L-
321 drain structures also facilitate water infiltration in soil with a low permeability (KS3) where groundwater velocities
322 are slightly higher than the base case model. Finally, it can be seen that slope accentuates groundwater velocity
323 differences along the transect. In the scenario where the hydraulic conductivity of the soil and the drain are high
324 (KS1 and KD1), the differences in groundwater velocity for the 10% and 30% slope scenarios increase.

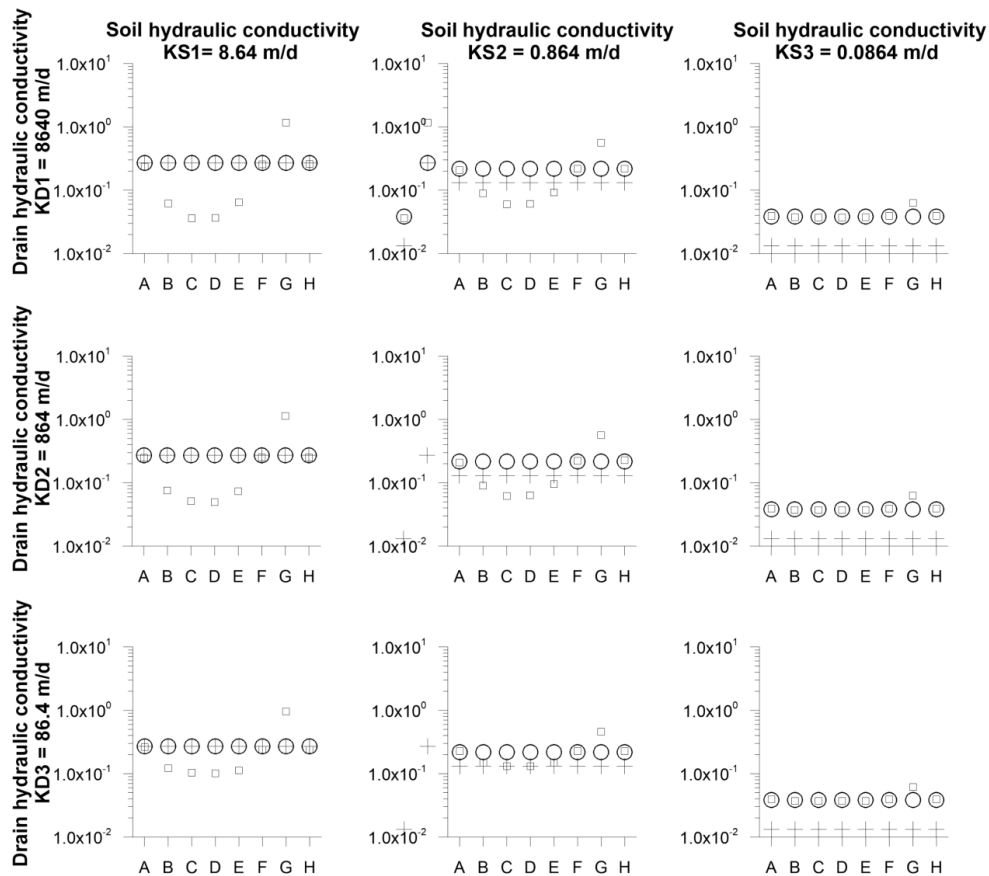
325 Results show that the no-excavation structure has the least impact on the groundwater velocities and the
326 wood-log structure has a limited impact on groundwater dynamics. The only difference with the base case (no road
327 at all) model is that the groundwater velocities observed are slightly higher where the hydraulic conductivity of
328 the soil layer is low (KS3). This is caused by the wood-log drain which facilitates water infiltration in a low-
329 conductive soil layer. Finally, the L-drain structure impacted significantly the groundwater dynamics. Significant
330 differences are observed in each scenario, mainly due to the L-shape drain. Downstream of the drain outlet
331 (observation point G), groundwater velocities are higher than other observation points along the transect,
332 regardless of the slope and the drain hydraulic conductivity. Maximum differences may reach two orders of
333 magnitude from 0.0346 (m/d) to 1.296 (m/d) in the same transect. Only the soil hydraulic conductivity reduces
334 differences in groundwater velocity along the transect and the slightly higher groundwater velocity in comparison
335 with the base case model indicates that gravel drain also facilitates water infiltration in low-conductivity soil layer.

336 The impact of the L-drain road structure which concentrates groundwater flow is clearly identified in the numerical
337 approach and is consistent with the field observations. For other road structures also, numerical models are
338 consistent with fieldwork results by showing a relatively undisturbed groundwater flow downslope the road. The
339 use of numerical models allowed for a quantitative estimation of the flow perturbation induced by each road
340 structure and model results were consistent with the field observations. In addition, the development of models
341 with various combinations of parameters also allowed for exploring a larger parameter space than using field work
342 only. For instance, the fact that the impact of an L-drain structure on the water dynamics is less marked if the
343 hydraulic conductivity of soil is low would have been impossible to identify by using fieldwork only.



344 The main simplification of the model is the assumption of a homogeneous hydraulic conductivity of the soil.
 345 Groundwater flow in fens can occur along preferential pathways. Therefore, the models are not able to reproduce
 346 small-scale processes, i.e. the exact hydraulic head in an individual mini-piezometer. Models results have to be
 347 interpreted as an average across multiple preferential flow paths.

348 Further investigations should be carried out to identify groundwater velocity threshold values above which a risk
 349 of for instance gully erosion is present. This is especially important for L-drain structures where the increase of
 350 flow velocities is higher than for the other structures. Finally, the impact on sloping fen vegetation related to
 351 perturbations of the groundwater flow should be further investigated. In this way, road construction could be better
 352 planned.

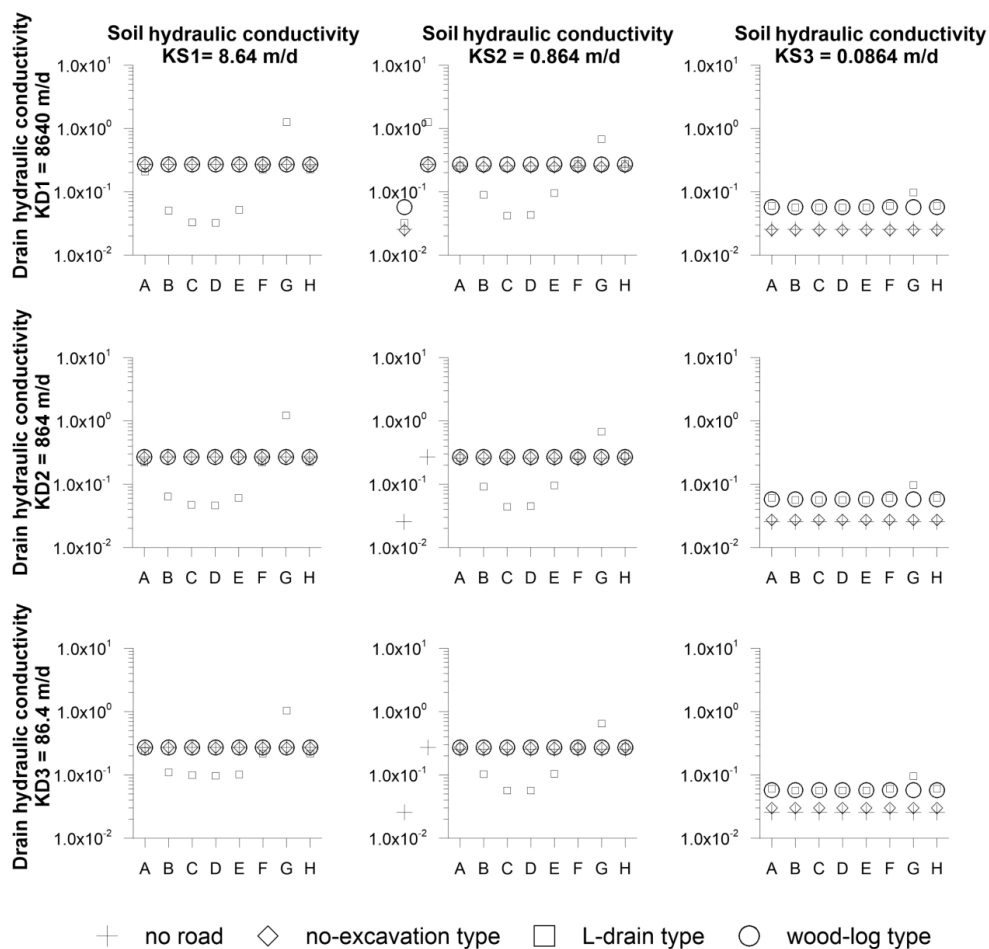


+ no road □ L-drain type ○ wood-log type

353

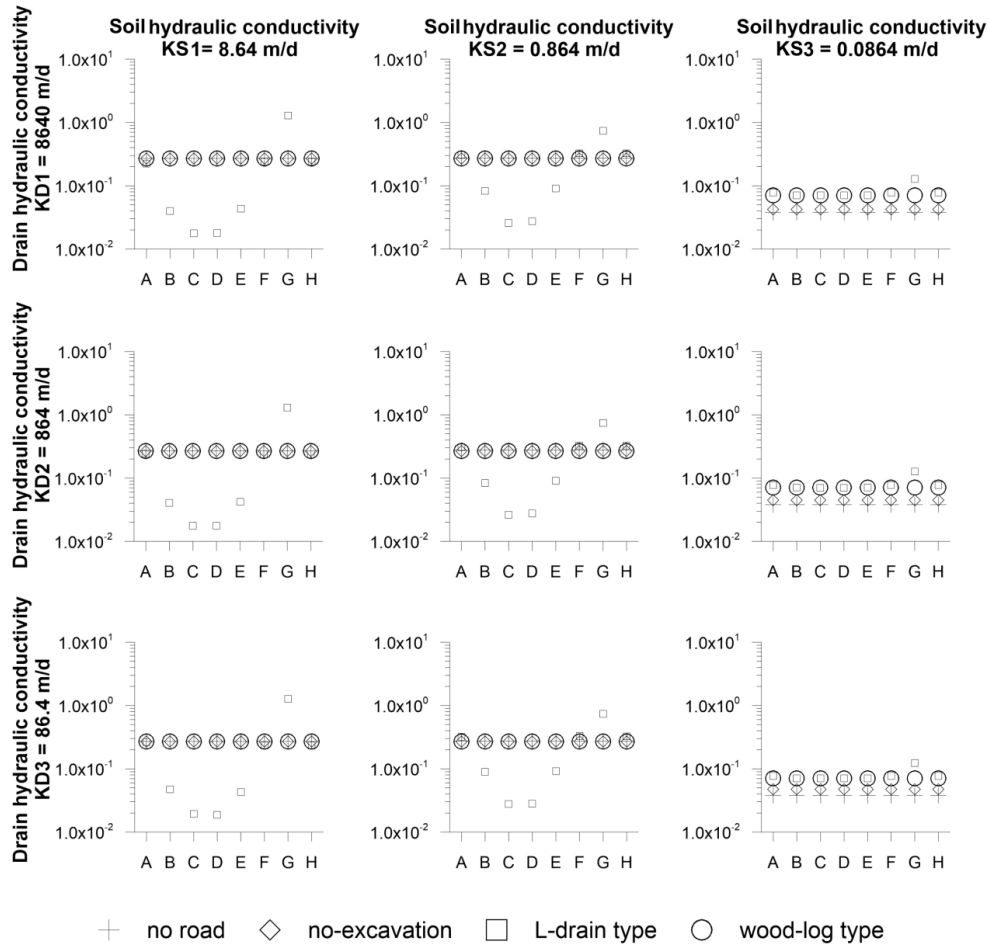


354 **Figure 8 : Simulated groundwater velocities downslope each road structures and each parameter combination with a**
 355 **slope of 10%.**



356

357 **Figure 9 : Simulated groundwater velocities downslope each road structures and each parameter combination with a**
 358 **slope of 20%.**



359

360 **Figure 10 : Simulated groundwater velocities downslope each road structures and each parameter combination with a**
 361 **slope of 30%.**

362 **4 Conclusions**

363 This study presented an assessment of three road structures regarding their perturbations of the natural
 364 groundwater flow. Two of these road structures were specifically developed to reduce the negative impacts of the
 365 road. The study is based on two complementary approaches; a tracer test in the field and numerical models
 366 simulating groundwater flow for the different road structures.

367 The tracer tests showed that both sides of all investigated road structures were hydraulically connected.
 368 Groundwater flow was heterogeneous suggesting the occurrence of preferential flow paths in the soil. The presence
 369 of a transversal drain (L-drain) beneath the road constitutes a preferential flow path, however, which is of much



370 greater importance than the naturally occurring preferential pathways. This was also confirmed by the models.
371 Velocities 10 times larger than in the natural case were obtained in the numerical simulations. This is not further
372 astonishing as the drains were specifically designed for this purpose. The two other road structures (wood-log and
373 no-excavation) do not perturb the flow field to the extent of the L-drain. To minimize the perturbation of flow
374 fields, the wood-log and no-excavation structures are recommended.

375 The combination of fieldwork and the development of numerical models was fundamental to achieve the
376 goal of this study. The tracer test allowed for a better understanding of groundwater flow throughout road structures
377 and allowed for evaluating their effectiveness at a given location. However, the tracer tests are time-consuming
378 and only a few field sites are available. The numerical approach, on the other hand, allows for exploring any
379 combination of slope, hydraulic properties or road structure, thus providing a more comprehensive approach. In
380 our study, the trends between the numerical and field approaches were consistent.

381 **5 Acknowledgements**

382 This research was funded by the Swiss Federal Office for the Environment (FOEN) and supported by Swiss
383 Federal Office for Agriculture (FOAG). The authors are grateful to Benoit Magnin, Peter Staubli Andreas Stalder,
384 Anton Stübi and Ueli Salvisberger for their collaborations.

385 **6 References**

386 Baker, C., Thompson, J. R. and Simpson, M.: 6. Hydrological Dynamics I: Surface Waters, Flood and
387 Sediment Dynamics The Wetlands Handbook, 1st edition. Edited by E. Maltby and T. Barker. 2009.
388 Blackwell Publishing, 120-168, 2009.

389 Betts, H. D., and DeRose, R. C.: Digital elevation models as a tool for monitoring and measuring gully
390 erosion, International Journal of Applied Earth Observation and Geoinformation, 1, 91-101,
391 [http://dx.doi.org/10.1016/S0303-2434\(99\)85002-8](http://dx.doi.org/10.1016/S0303-2434(99)85002-8), 1999.

392 Broggi, M. E.: Minimum requis de surfaces proches de l'état naturel dans le paysage rural, illustré par
393 l'exemple du Plateau suisse. Liebefeld-Berne., Rapport 31a du Programme national de recherche "Sol",
394 199p, 1990.

395 Brunner, P., and Simmons, C. T.: HydroGeoSphere: a fully integrated, physically based hydrological
396 model, Groundwater, 50, 170-176, 2012.

397 Capra, A., Porto, P., and Scicolone, B.: Relationships between rainfall characteristics and ephemeral
398 gully erosion in a cultivated catchment in Sicily (Italy), Soil and Tillage Research, 105, 77-87,
399 <http://dx.doi.org/10.1016/j.still.2009.05.009>, 2009.

400 Charman, D.: Peatlands and environmental change. John Wiley & Sons Ltd. 301 2002.



- 401 Chimner, R. A., Cooper, D. J., Wurster, F. C. and Rochefort, L.: An overview of peatland restoration in
402 North America: where are we after 25 years?, *Restoration Ecology*, 25, 283-292, 2016.
- 403 Cognard Plancq, A. L., Bogner, C., Marc, V., Lavabre, J., Martin, C., and Didon Lescot, J. F.: Etude du rôle
404 hydrologique d'une tourbière de montagne: modélisation comparée de couples "averse-crue" sur deux
405 bassins versants du Mont-Lozère., *Etudes de géographie physique*, n° XXXI, p. 3 - 15, 2004.
- 406 Daba, S., Rieger, W., and Strauss, P.: Assessment of gully erosion in eastern Ethiopia using
407 photogrammetric techniques, *CATENA*, 50, 273-291, [http://dx.doi.org/10.1016/S0341-
408 8162\(02\)00135-2](http://dx.doi.org/10.1016/S0341-8162(02)00135-2), 2003.
- 409 Derose, R. C., Gomez, B., Marden, M., and Trustrum, N. A.: Gully erosion in Mangatu Forest, New
410 Zealand, estimated from digital elevation models, *Earth Surface Processes and Landforms*, 23, 1045-
411 1053, 10.1002/(SICI)1096-9837(1998110)23:11<1045::AID-ESP920>3.0.CO;2-T, 1998.
- 412 Descroix, L., González Barrios, J. L., Viramontes, D., Poulenard, J., Anaya, E., Esteves, M., and Estrada,
413 J.: Gully and sheet erosion on subtropical mountain slopes: Their respective roles and the scale effect,
414 *CATENA*, 72, 325-339, <http://dx.doi.org/10.1016/j.catena.2007.07.003>, 2008.
- 415 Dutton, A. L., Loague, K., and Wemple, B. C.: Simulated effect of a forest road on near-surface
416 hydrologic response and slope stability, *Earth Surface Processes and Landforms*, 30, 325-338,
417 10.1002/esp.1144, 2005.
- 418 Li, Q., Unger, A. J. A., Sudicky, E. A., Kassenaar, D., Wexler, E. J., and Shikaze, S.: Simulating the multi-
419 seasonal response of a large-scale watershed with a 3D physically-based hydrologic model, *Journal of*
420 *Hydrology*, 357, 317-336, <http://dx.doi.org/10.1016/j.jhydrol.2008.05.024>, 2008.
- 421 Limpens, J., Berendse, F., Blodau, C., Canadell, J. G., Freeman, C., Holden, J., Roulet, N., Rydin, H. and
422 Schaepman-Strub, G.: Peatlands and the carbon cycle: from local processes to global implications – a
423 synthesis, *Biogeosciences*, 5, 1475-1491, 2008.
- 424 Lindsay, R.: Peatbogs and carbon: a critical synthesis to inform policy development in oceanic peat bog
425 conservation and restoration in the context of climate change, University of East London, Technical
426 Report, 2010.
- 427 Loague, K., and VanderKwaak, J. E.: Simulating hydrological response for the R-5 catchment:
428 comparison of two models and the impact of the roads, *Hydrological Processes*, 16, 1015-1032,
429 10.1002/hyp.316, 2002.
- 430 Martínez-Casasnovas, J. A.: A spatial information technology approach for the mapping and
431 quantification of gully erosion, *CATENA*, 50, 293-308, [http://dx.doi.org/10.1016/S0341-
432 8162\(02\)00134-0](http://dx.doi.org/10.1016/S0341-8162(02)00134-0), 2003.
- 433 Nyssen, J., Poesen, J., Moeyersons, J., Luyten, E., Veyret-Picot, M., Deckers, J., Haile, M., and Govers,
434 G.: Impact of road building on gully erosion risk: a case study from the Northern Ethiopian Highlands,
435 *Earth Surface Processes and Landforms*, 27, 1267-1283, 10.1002/esp.404, 2002.
- 436 Poesen, J., Nachtergaele, J., Verstraeten, G., and Valentin, C.: Gully erosion and environmental change:
437 importance and research needs, *CATENA*, 50, 91-133, [http://dx.doi.org/10.1016/S0341-
438 8162\(02\)00143-1](http://dx.doi.org/10.1016/S0341-8162(02)00143-1), 2003.



- 439 Reckendorfer, W., Funk, A., Gschöpf, C., Hein, T. and Schiemer, F.: Aquatic ecosystem functions of an
440 isolated floodplain and their implications for flood retention and management, *Journal of Applied*
441 *Ecology*, 50, 119–128, 2013.
- 442 Reid, L. M., and Dunne, T.: Sediment production from forest road surfaces, *Water Resources Research*,
443 20, 1753-1761, [10.1029/WR020i011p01753](https://doi.org/10.1029/WR020i011p01753), 1984.
- 444 Rydin, H. a. J., J.: *The biology of peatlands*, Oxford University Press, 343p., 2005.
- 445 Samaritani, E., Siegenthaler, A., Yli-Petäys, M., Buttler, A., Christin, P.-A., and Mitchell, E. A. D.: Seasonal
446 Net Ecosystem Carbon Exchange of a Regenerating Cutaway Bog: How Long Does it Take to Restore
447 the C-Sequestration Function?, *Restoration Ecology*, 19, 480-489, [10.1111/j.1526-100X.2010.00662.x](https://doi.org/10.1111/j.1526-100X.2010.00662.x),
448 2011.
- 449 Therrien, R., Sudicky, E. A., McLaren, R. G., and Panday, S. M.: HydroGeoSphere. A three-dimensional
450 numerical model describing fully-integrated subsurface and surface flow and solute transport, 5, 343,
451 2005.
- 452 Valentin, C., Poesen, J., and Li, Y.: Gully erosion: Impacts, factors and control, *CATENA*, 63, 132-153,
453 [http://dx.doi.org/10.1016/j.catena.2005.06.001](https://doi.org/10.1016/j.catena.2005.06.001), 2005.
- 454 Van Genuchten, M. T.: A closed-form equation for predicting the hydraulic conductivity of unsaturated
455 soils, *Soil science society of America journal*, 44, 892-898, 1980.
- 456 VanderKwaak, J. E.: Numerical simulation of flow and chemical transport in integrated surface-
457 subsurface hydrologic systems, Ph.D. thesis, Departement of Earth Science, University of Waterloo,
458 Waterloo, Ontario, Canada., 1999.
- 459 von Sengbusch, P.: Enhanced sensitivity of a mountain bog to climate change as a delayed effect of
460 road construction, *Mires and Peat*, 15: Art. 6, (Online: [http://www.mires-and-](http://www.mires-and-peat.net/pages/volumes/map15/map1506.php)
461 [peat.net/pages/volumes/map15/map1506.php](http://www.mires-and-peat.net/pages/volumes/map15/map1506.php)), 2015.
- 462 Wemple, B. C., and Jones, J. A.: Runoff production on forest roads in a steep, mountain catchment,
463 *Water Resources Research*, 39, 2003.
- 464 Zollner, A.: Das Abflussgeschehen von unterschiedlich genutzten Hochmooreinzugsgebieten - Bayer.
465 Akad. f. Naturschutz u. Landschaftspflege - Laufen / Salzach, Laufener Seminarbeitr., 111-119, 2003.
- 466